ARTICLES
https://doi.org/10.1038/s41561-017-0007-2
nature geoscience

Links between sediment consolidation and Cascadia megathrust slip behaviour

Shuoshuo Han[1*], Nathan L. Bangs[1], Suzanne M. Carbotte[2], Demian M. Saffer[3] and James C. Gibson[2]

At sediment-rich subduction zones, megathrust slip behaviour and forearc deformation are tightly linked to the physical properties and in situ stresses within underthrust and accreted sediments. Yet the role of sediment consolidation at the onset of subduction in controlling the downdip evolution and along-strike variation in megathrust fault properties and accretionary wedge structure is poorly known. Here we use controlled-source seismic data combined with ocean drilling data to constrain the sediment consolidation and in situ stress state near the deformation front of the Cascadia subduction zone. Offshore Washington where the megathrust is inferred to be strongly locked, we find over-consolidated sediments near the deformation front that are incorporated into a strong outer wedge, with little sediment subducted. These conditions are favourable for strain accumulation on the megathrust and potential earthquake rupture close to the trench. In contrast, offshore Central Oregon, a thick under-consolidated sediment sequence is subducting, and is probably associated with elevated pore fluid pressures on the megathrust in a region where reduced locking is inferred. Our results suggest that the consolidation state of the sediments near the deformation front is a key factor contributing to megathrust slip behaviour and its along-strike variation, and it may also have a significant role in the deformation style of the accretionary wedge.

The Cascadia subduction zone is unusually quiet, with few instrumentally recorded earthquakes on the plate interface. However, palaeoseismic studies indicate that this margin has hosted M_w 8–9 megathrust earthquakes at 200–530-yr intervals during the Holocene epoch with persistent rupture segment boundaries[1–3] (Fig. 1). The last M_w ~9 event occurred in 1700 and produced a transoceanic tsunami recorded in Japan[4]. Land-based geodetic observations indicate that a mostly locked megathrust lies largely offshore, and exhibits along-strike variation in the extent of locking[5–8]. In existing models, the plate interface offshore Washington is strongly locked, whereas Central Oregon between 43° N and 46° N is characterized by reduced inter-seismic uplift and co-seismic subsidence, suggesting that a significant portion of plate convergence is taken up by aseismic slip there[6–8] (Fig. 1). The shallow portion of the megathrust lies beneath an accretionary wedge that is wide offshore of North Oregon and Washington where it is characterized by dominantly landward-vergent thrust faults[9–12], but is narrow offshore of Vancouver Island, Central/South Oregon and North California where there are dominantly seaward-vergent thrust faults, or mixed-vergent faults in the case of North California[13] (Fig. 1 and Supplementary Fig. 1).

The ability of the shallow-most megathrust to accumulate strain depends on its physical properties, while its potential to rupture co-seismically depends on the in situ stress along the fault and within the outer accretionary wedge, both of which are closely tied to the consolidation state of the accreted and underthrust sediments. At Cascadia, little is known about initial sediment consolidation near the deformation front and its downdip and along-strike variations. Early studies that used seismic velocity to constrain sediment consolidation[14–16] sampled two local zones off Vancouver Island and Oregon with comparatively poor resolution of sediment properties due to the short source–receiver offset (3.6 km) and the processing methods used. Here we derive P-wave velocity (V_p) models for the sediment section through pre-stack depth migration (PSDM) from long source–receiver offset (8 km) multichannel seismic data collected during the 2012 Juan de Fuca Ridge-to-Trench Experiment[17,18]. We focus on two cross-margin transects that sample the strongly locked Washington region (47.4° N) and the potentially partially creeping Central Oregon region (44.6° N), and an along-margin north–south transect extending from 44.3° N to 47.8° N (Fig. 1). We integrate these results with rock physics models calibrated by ocean drilling data from the Juan de Fuca Plate to quantify the sediment consolidation state and estimate in situ stress conditions near the deformation front and in the outer wedge (Methods and Supplementary Information).

Sediment consolidation offshore Washington and Oregon

Our PSDM V_p models and velocity-derived estimates of in situ porosity document the evolution of sediment properties from the incoming plate into the outer portion of the subduction zone, and reveal contrasting consolidation and effective stress states along the margin in regions of similar sediment thickness (Figs. 2 and 3). The seismic velocities of the incoming sediments ~ 30 km seaward from the deformation front are similar on the WA and OR transects (Fig. 2a,b) and are consistent with a normally consolidated reference velocity profile expected for sedimentation-driven burial (Supplementary Fig. 2 and Methods). On the WA transect, over-consolidation (positive residual V_p) starts to develop ~ 20 km seaward of the deformation front (Fig. 2c). Near the deformation front, where a landward-vergent frontal thrust dipping ~30° extends through the sediment section and shoals into a décollement ~170 m above the basement (Fig. 1b and Supplementary Fig. 1), a positive residual V_p is observed in the entire sediment sequence and reaches 0.6–0.8 km s^{-1} near the basement (Fig. 2c). The sediments are further consolidated in the outer wedge (Fig. 2a,c), where landward-vergent thrust faults dipping 25°–35° extend close to the basement and indicate that very little of the incoming sediment is subducting (Fig. 1b and Supplementary Fig. 1).

[1]Institute for Geophysics, Jackson School of Geosciences, The University of Texas at Austin, Austin, TX, USA. [2]Lamont-Doherty Earth Observatory, Columbia University, Palisades, NY, USA. [3]Department of Geosciences and Center for Geomechanics, Geofluids, and Geohazards, The Pennsylvania State University, University Park, PA, USA. *e-mail: han@ig.utexas.edu

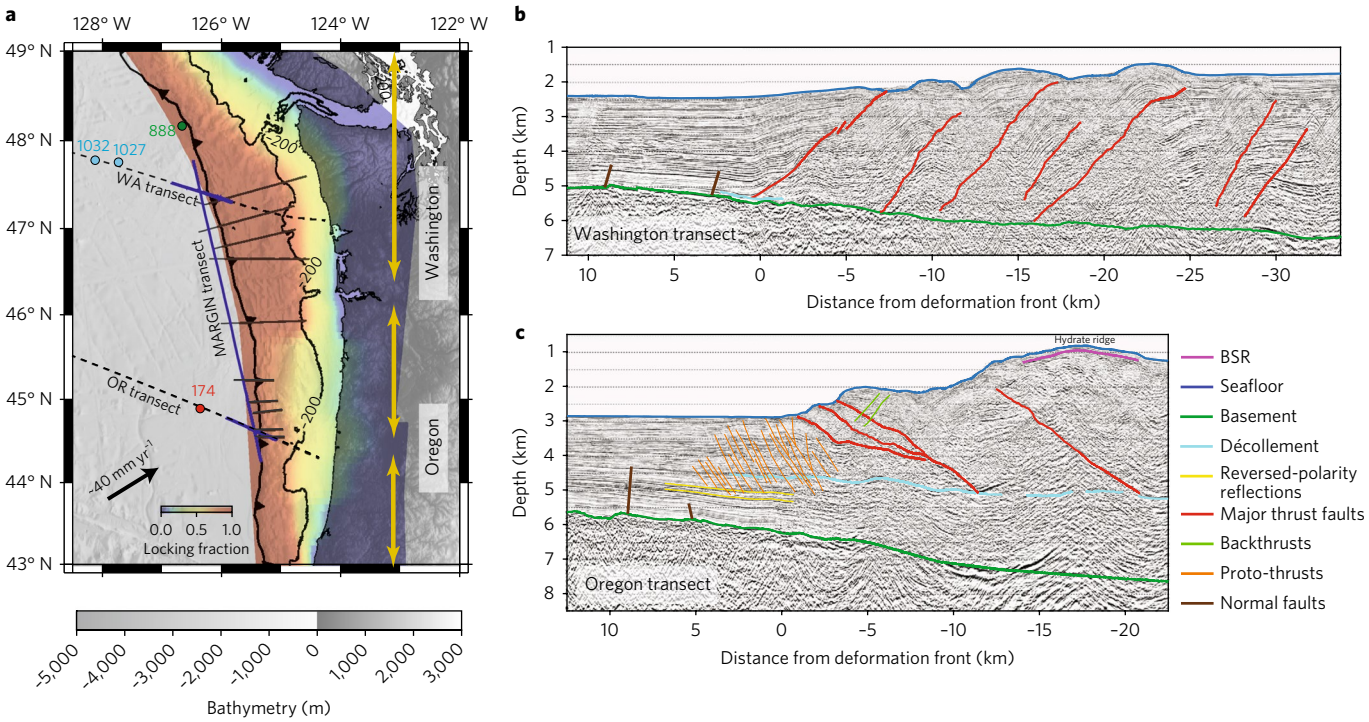

Fig. 1 | Palaeo-earthquake rupture segments and current megathrust locking status of the Cascadia subduction zone, and representative forearc structures offshore Washington and Central Oregon. a, Regional map of the Cascadia subduction zone superimposed by extent of palaeo-earthquake rupture segments[3] (thick yellow bars) and current megathrust locking fraction[8]. Accretionary wedge is bounded by deformation front (barbed thick black lines) and 200 m depth contour (thin black line). The dashed black lines show seismic transects from the Juan de Fuca Ridge-to-Trench experiment, with the data subset used in this study in thick blue lines. The thin grey lines show previous published seismic transects[9–12] from which underthrust sediment thickness is compiled (Supplementary Table 1). The coloured circles denote locations of Deep Sea Drilling Program/Ocean Drilling Program drilling sites[45–47]. The convergence vector is represented by a black arrow. **b**,**c**, Interpreted pre-stack depth-migrated seismic reflection images of WA and OR transects near the deformation front. Vertical exaggeration is 2:1. See Supplementary Fig. 1 for un-interpreted images.

In contrast, offshore Central Oregon, the topmost 1.5–1.7 km of the incoming sediment become progressively over-consolidated towards the deformation front, with a group of seaward-vergent proto-thrusts (dips 35°–45°) imaged above horizons with reversed-polarity reflections[15]; yet sediments below are under-consolidated (negative residual V_p) (Figs. 1c and 2d, and Supplementary Fig. 1). Approaching the deformation front, V_p in the basal sediment (100–500 m above the basement) is essentially unchanged despite increasing burial depth, leading to increasingly negative residual V_p (Fig. 2b,d). The basal sediment V_p near the deformation front is significantly lower than along the WA transect at the same depth (3.3–3.6 km s^{-1}, compared with 4.0–4.2 km s^{-1}) (Fig. 2a,b). Shallowly dipping (~20°) frontal thrusts merge with a décollement reflection that is ~1.7 km above basement near the deformation front and can be traced landward beneath Hydrate Ridge (Fig. 1c and Supplementary Fig. 1). The underthrust sediments below the décollement remain under-consolidated, whereas the accreted sediments above remain over-consolidated (Fig. 2d). Comparison between the two transects shows that the basal sediments on the OR transect maintain a relatively high porosity (8–14%) near the deformation front and beneath the outer wedge (Fig. 2e), and support a low mean effective stress, ~60–80% of that experienced by basal sediments on the WA transect (Fig. 2g). Sediments above the décollement in the accretionary wedge offshore Oregon also have, on average, higher porosity and lower mean effective stress than those in the Washington wedge (Fig. 2f,h).

Variations in basal sediment velocity along our MARGIN transect reveal the evolution of sediment consolidation state between the OR and WA transects and its relationship to variations in the depth of the décollement (compiled from this study and existing seismic data[9–12,18]; Fig. 3 and Supplementary Table 1). Along the southern portion of the MARGIN transect where the décollement is ~1.4–1.7 km above the basement, the residual V_p of the basal sediment is generally zero to negative, indicating normal to under-consolidation. The residual V_p switches to positive, indicative of over-consolidation, near 45° N, where the décollement steps down to 0.4 km above the basement crossing the Daisy Bank strike-slip fault[9,10] (Fig. 3). This location also marks a prominent change in forearc structure from dominantly seaward-vergent to landward-vergent thrust faults[9,10] with a reduction in wedge taper. Further north, where the décollement remains <0.6 km above the basement[11,12], the residual basal sediment V_p is mostly positive, indicative of over-consolidation (Fig. 3).

Impacts on megathrust slip behaviour

Our observations from the OR, WA and MARGIN transects indicate that distinct sediment consolidation patterns develop near the deformation front and in the outer wedge, and are related to the depth of the décollement. Offshore Washington where the décollement lies near the basement, the entire sedimentary section is subjected to horizontal compression from the accretionary wedge, even 10–15 km seaward of the trench, leading to over-consolidation. These over-consolidated and strengthened sediments are then incorporated into the wedge and further consolidated. With little subducted fluid-rich sediments and a relatively strong accretionary wedge, the Washington megathrust is likely to be mechanically strong[19]. In contrast, offshore Central Oregon where the décollement is shallower, the thick subducting sediment section is shielded from horizontal compression in the wedge above and is subjected

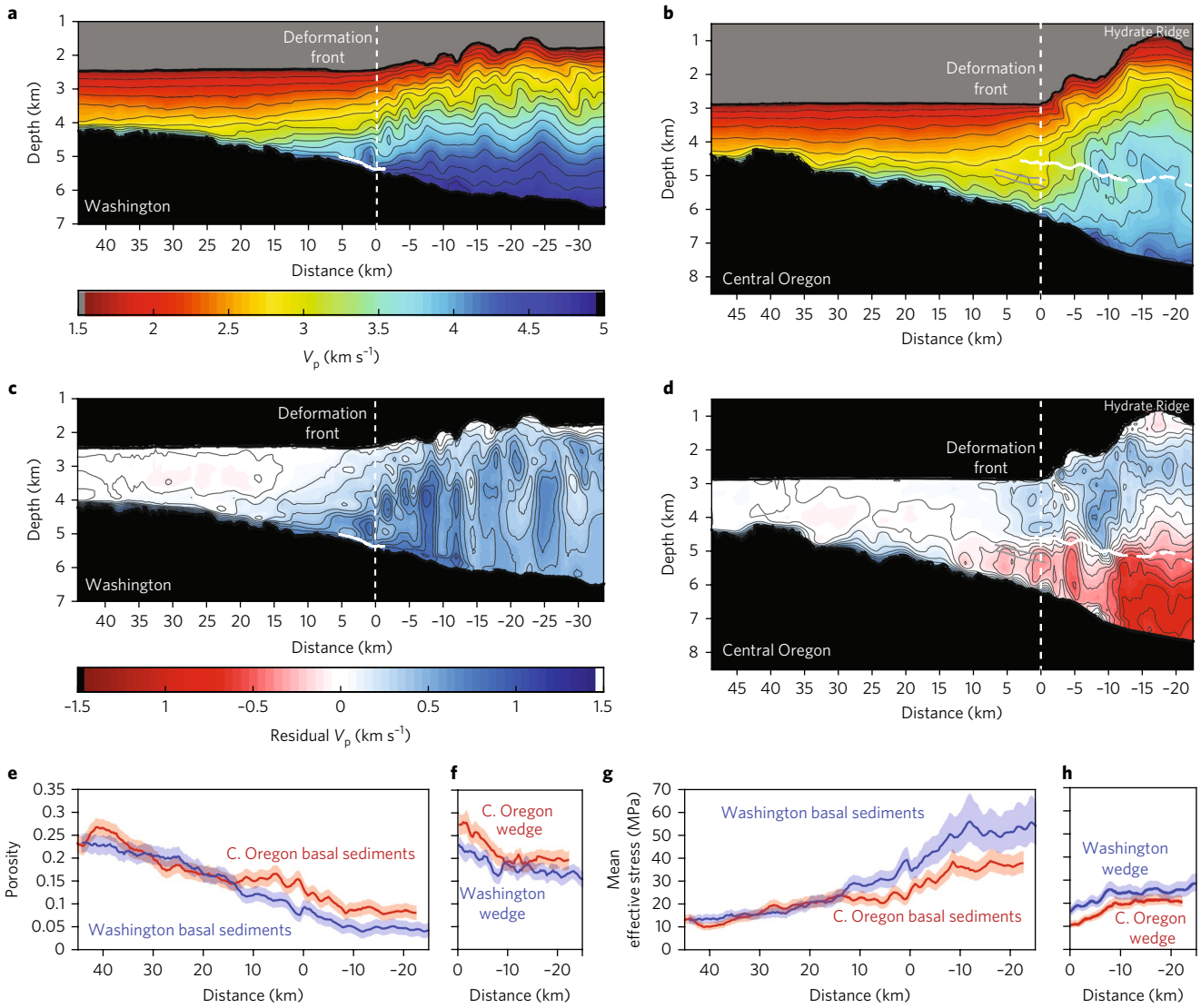

Fig. 2 | Comparison of sediment consolidation and in situ stress state between the Washington transect (47.4° N) and the Oregon transect (44.6° N). **a**,**b**, Pre-stack depth-migration P-wave velocity (V_p) models of the WA and OR transects. Décollements are indicated by thick white lines. Horizons with reversed-polarity reflections are indicated by grey lines. The vertical white dashed lines mark the deformation front. **c**,**d**, Residual V_p relative to predicted normal consolidation V_p profile (Supplementary Fig. 2). **e**–**h**, Average porosity (**e**,**f**) and mean effective stress (**g**,**h**) of basal sediments (100–500 m above the basement) and wedge sediments. The pale blue and red shades represent the uncertainty of the porosity and mean effective stress associated with ±5% of the seismic velocity uncertainty for the WA and OR transects.

to less stress in comparison with sediments at the same depths off Washington. With the delayed consolidation, high porosity is maintained in this section, probably resulting from trapped fluids due to a combination of rapid burial and low permeability, such that drainage does not keep pace with loading. With the warm thermal state of Cascadia, mineral dehydration reactions may occur outboard of the trench[20], and the released fluid may also contribute to elevated pore pressures. Yet as the V_p and inferred porosity in the basal sediment is approximately constant approaching the deformation front (Fig. 2b,e), which could be explained by delayed consolidation, addition of a large amount of fluid from dehydration reactions is not required by our data. Some of the proto-thrust faults extend through the horizons with reversed-polarity reflections in the lower sediment section (Fig. 1c and Supplementary Figs. 1 and 4b), and could provide effective pathways for the local drainage of the trapped fluid[21], and thus may account for the small-scale lateral variations in the inferred porosity of basal sediments seaward of the deformation front (Fig. 2b,d). The overall high fluid content in the subducting sediments probably facilitates elevated pore pressure on the plate interface, and thus potentially weakens the megathrust. The small horizontal stresses associated with this weak basal décollement would, in turn, lead to smaller horizontal compressive stresses and less consolidation within the wedge[22].

Our observations of along-strike variation in sediment consolidation state and its implications for the strength of the megathrust correlate broadly with variations in inter-seismic locking of the Cascadia megathrust inferred from geodetic observations[6–8]. Although current locking models are based on onshore data, thus lacking resolution in the near-trench region, the models all indicate that Central Oregon has a narrower locking zone or reduced locking fraction in comparison with Washington[5–8]. In our study area offshore Central Oregon, we observe a thick layer of fluid-rich sediments subducting beneath the shallow portion of the megathrust, providing favourable conditions for the development of high fluid pressures at the plate interface[23,24]. Further downdip, a nearby magnetotelluric transect reveals high electrical conductivity near

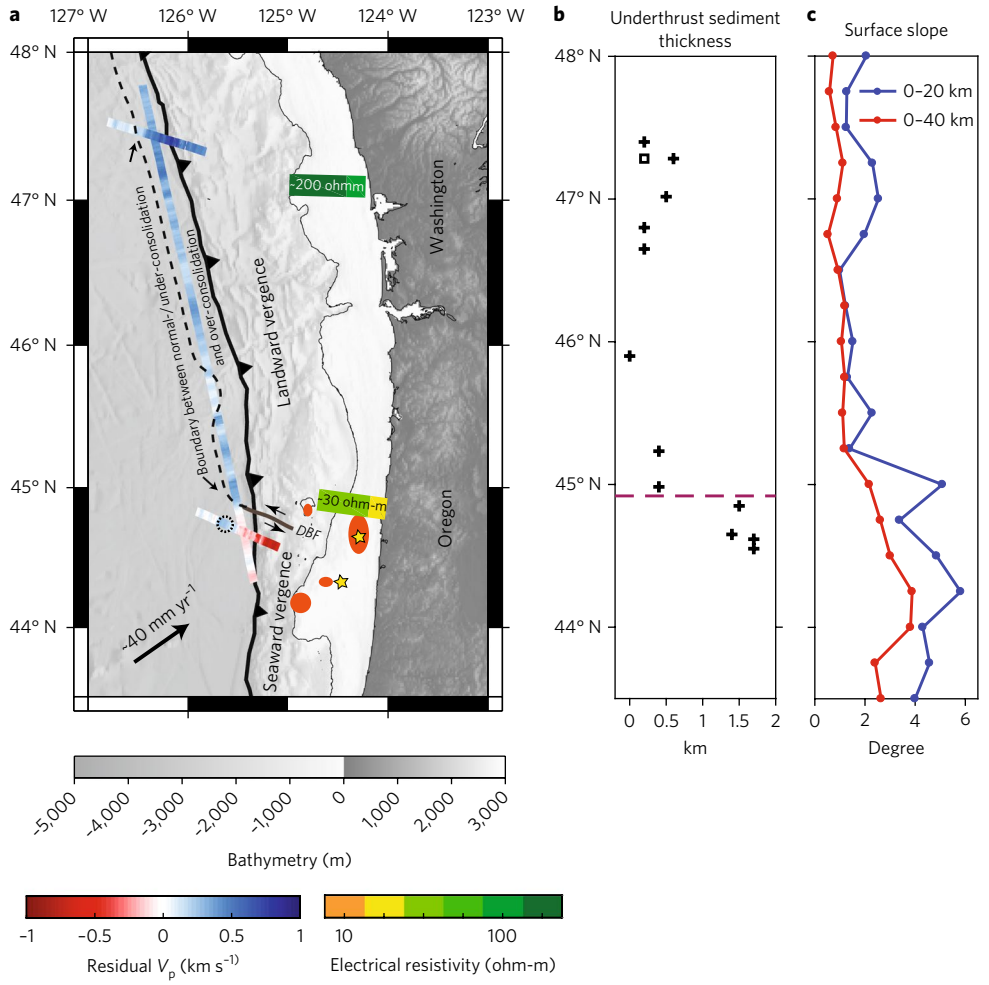

Fig. 3 | Along-strike variation in sediment consolidation state in relation to underthrust sediment thickness and forearc structure from 44.3° N to 47.8° N. a, Residual V_p of the basal sediment along the WA, OR and MARGIN transects with interpreted boundary between normal-/under-consolidated and over-consolidated sediments (black dashed line). The black dashed circle marks the anomalous over-consolidated basal sediments between 14 and 27 km on the OR transect, which may be related to effective drainage of fluid by large-offset subduction bending normal faults in this area[18]. The thick coloured bars denote plate-interface electrical resistivity[25]. The orange ellipses show the magnetic and gravity anomalies from which subducted seamounts are inferred[36]. The yellow stars mark the locations of repeated earthquake swarms[36]. Dominant vergence of thrust faults in the accretionary wedge across the Daisy Bank Fault (DBF) (brown line) are labelled. **b**, Underthrust sediment thickness (shown by crosses) near the deformation front (see compilation in Supplementary Table 1). Square: reinterpretation of seismic images of ORWELL Line 103[11] by this study. **c**, Surface slope of the outermost 20 km and 40 km of accretionary wedge. See Supplementary Fig. 3 for locations of bathymetry profiles.

the plate interface extending to the coast that has been attributed to subducted sediments and associated dewatering[25] (Fig. 3a). The thick subducted sediment layer and expected high pore fluid pressure and low effective stress across the Central Oregon megathrust probably play an important role in facilitating the aseismic slip inferred in this region[26,27]. In contrast, offshore Washington where we observe very little subducted sediment, magnetotelluric data show an electrically resistive plate interface beneath the continental shelf[25], consistent with the higher degree of inferred megathrust locking there[6–8] (Fig. 3a). It is noteworthy that along the Hikurangi margin, a transition of megathrust slip behaviour from weak interseismic locking and shallow slow-slip in the north to strong locking in the south is well documented[28]. Similar to our observations at Cascadia, significant sediment subduction and associated elevated pore fluid pressure are inferred from high electrical conductivity and high V_p/V_s ratios near the plate interface of the weakly locked northern Hikurangi megathrust, but are absent in the south[29,30].

Sediment consolidation state near the deformation front and in the outer wedge also has important implications for earthquake rupture at Cascadia. Palaeoseismic studies indicate a rupture segment spanning Washington with the longest earthquake recurrence interval (500–530 yr)[3] along the Cascadia margin, and a segment spanning South–Central Oregon that ruptures more often (300–380 yr)[3], consistent with the different décollement strength inferred from our study (Fig. 1). Our observations of high V_p and large effective stress in the Washington outer wedge indicate a strong sediment section. A similarly competent accretionary wedge has been inferred from high V_p and well-preserved sediment stratigraphy[31,32] in the region of the 2004 M_w 9.2 Sumatra earthquake where co-seismic rupture propagated ~1,300 km along-strike, and possibly extended to the trench[32,33]. This inference is supported by recent ocean drilling of the incoming sediments outboard North Sumatra, which shows that mechanical compaction and diagenesis have significantly increased the strength of the sediment section prior to subduction[34]. The elastic properties of the high-V_p wedge and strengthened basal sediments would support greater strain accumulation and more effective transmission of elastic stresses during rupture, and thus may contribute to extending the seismogenic zone seaward to the shallow outer forearc

and facilitate rupture over long distances[34]. As the updip limit and along-strike distance of megathrust rupture is closely related to maximum earthquake magnitude and tsunamigenic potential, the over-consolidated sediments we find off Washington indicate enhanced earthquake and tsunami hazard in this region.

It is intriguing that the depth of décollement, which exerts key control on sediment consolidation state, is markedly different offshore Washington and Central Oregon, despite similar incoming sediment thickness (Figs. 1b,c and 3b). The different décollement levels may reflect the presence/absence of layers with intrinsic frictional weakness or low permeability in the sediment sections off Central Oregon and Washington. South of 45° N, the shallow décollement projects to either the interpreted boundary between the Astoria Fan turbidites and the abyssal plain turbidites or a level several hundred metres below it[9,10,15,16], which may correspond to a major lithological and permeability change that would trap fluid pressures and thus weaken this interval[35] (Supplementary Fig. 1). Seamount subduction may also play an important role in the formation of the shallow décollement off Central Oregon. Between 44°N and 45° N, where repeated clusters of small earthquakes are recorded, a group of buried seamounts is identified based on magnetic and gravity anomalies[36] (Fig. 3a). Farther south, three large-scale continental slope failures between 42.3° and 44.2° N have been attributed to collision of a seamount province or an aseismic ridge[37]. Recent numerical simulations demonstrate that as a seamount subducts, the décollement can shift to a shallower depth if there is a weak horizon available to exploit and thus perpetuate shallow initiation of the megathrust at the deformation front[38]. Elevated pore pressure can also develop along the plate interface several tens of kilometres downdip of the subducted seamounts, as observed along the Hikurangi margin[39]. We speculate that the shallow décollement at Central Oregon is linked to subduction of seamounts distributed throughout this region. Once a shallow décollement is formed, the thick under-consolidated, fluid-rich sediment sequence subducting beneath Central Oregon contributes to maintain a relatively weak megathrust.

Contributions to forearc deformation

Sediment consolidation state also coincides with along-strike changes in forearc deformation style. North of 45° N where over-consolidated sediments are present near the deformation front, the forearc wedge has a low taper angle (surface slope: 1°–2.5°, basal slope at the top of oceanic crust: ~2°–3°) and is characterized by landward-vergent thrust faults[9–12] (Fig. 3). South of 45° N where normal- and under-consolidated sediments are subducting, the outer wedge is of relatively high taper angle (surface slope: 2°–6°, basal slope at décollement: 2°–3°) with seaward-vergent thrust faults[9–12,15,16] (Fig. 3). The formation mechanism of the atypical landward-vergent thrust faults is poorly understood. Existing hypotheses, based mostly on analogue and numerical modeling, include: a frictionally weak décollement, a thick ductile basal layer, a strong wedge, a seaward-dipping backstop, dynamic weakening of the megathrust during earthquakes and strong lateral wall effects from strike-slip faults[9,40–42]. Among these hypotheses, a weak basal layer related to pore fluid over-pressure is the most frequently invoked. Our observations at Washington of an over-consolidated wedge and no resolvable low-velocity layer near the basement argue against the basal-layer mechanisms, and highlight the importance of a strong wedge in forming these atypical faults. At Sumatra, the other primary location where landward vergent faults are well described, the properties of the wedge are remarkably similar, with a thick incoming sediment section (over 4 km), a décollement that lies near the basement, and average low taper angles (including a steep toe and plateau geometry)[31,32,43]. At both locations, a stiff and strong wedge resulting from sediment over-consolidation that begins outboard of the trench may play a key role in the formation of landward-vergent faults and may contribute to generating large tsunamis in these regions[41].

As shown in numerous observational and experimental studies, fluid plays a key role in fault slip behaviour[23,24,44]. The amount and the consolidation state of sediments entering subduction zones directly impact the fluid content near the megathrust, and strongly influence the mechanical strength of the plate interface and outer wedge. Our study finds contrasting sediment consolidation states offshore of Washington and Central Oregon that are linked to the along-strike variations inferred in inter-seismic locking and co-seismic rupture of the Cascadia megathrust. Our work also demonstrates that physical properties and in situ stresses of incoming, accreted and underthrust sediments near the deformation front potentially influence megathrust properties, and thus slip behaviour, tens of kilometres downdip. Understanding consolidation state near the deformation front potentially offers clues to earthquake and tsunami hazards in other sediment-rich subduction zones, such as Eastern Aleutian, Central–South Chile, Sumatra and Makran.

Received: 2 March 2017; Accepted: 11 October 2017;
Published online: 20 November 2017

References

1. Atwater, B. F. Evidence for great Holocene earthquakes along the outer coast of Washington-state. *Science* **236**, 942–944 (1987).
2. Adams, J. Paleoseismicity of the Cascadia subduction zone: Evidence from turbidites off the Oregon-Washington margin. *Tectonics* **9**, 569–583 (1990).
3. Goldfinger, C. et al. *Turbidite Event History — Methods and Implications for Holocene Paleoseismicity of the Cascadia Subduction Zone* US Geological Survey Professional Paper 1661–F (USGS, 2012).
4. Satake, K., Wang, K. & Atwater, B. F. Fault slip and seismic moment of the 1700 Cascadia earthquake inferred from Japanese tsunami descriptions. *J. Geophys. Res.* **108**, 2535 (2003).
5. Wang, K., Wells, R., Mazzotti, S., Hyndman, R. D. & Sagiya, T. A revised dislocation model of interseismic deformation of the Cascadia subduction zone. *J. Geophys. Res.* **108**, 2026 (2003).
6. Burgette, R. J., Weldon, R. J. & Schmidt, D. A. Interseismic uplift rates for western Oregon and along-strike variation in locking on the Cascadia subduction zone. *J. Geophys. Res.* **114**, B01408 (2009).
7. McCaffrey, R., King, R. W., Payne, S. J. & Lancaster, M. Active tectonics of northwestern US inferred from GPS-derived surface velocities. *J. Geophys. Res.* **118**, 709–723 (2013).
8. Schmalzle, G. M., McCaffrey, R. & Creager, K. C. Central Cascadia subduction zone creep. *Geochem. Geophys. Geosyst.* **15**, 1515–1532 (2014).
9. Mackay, M. E., Moore, G. F., Cochrane, G. R., Moore, J. C. & Kulm, L. D. Landward vergence and oblique structural trends in the oregon margin accretionary prism — implications and effect on fluid-flow. *Earth Planet. Sci. Lett.* **109**, 477–491 (1992).
10. MacKay, M. E. Structural variation and landward vergence at the toe of the Oregon accretionary prism. *Tectonics* **14**, 1309–1320 (1995).
11. Adam, J., Klaeschen, D., Kukowski, N. & Flueh, E. Upward delamination of Cascadia Basin sediment infill with landward frontal accretion thrusting caused by rapid glacial age material flux. *Tectonics* **23**, (2004).
12. Booth-Rea, G., Klaeschen, D., Grevemeyer, I. & Reston, T. Heterogeneous deformation in the Cascadia convergent margin and its relation to thermal gradient (Washington, NW USA). *Tectonics* **27**, TC4005 (2008).
13. Gulick, S. P. S., Meltzer, A. M. & Clarke, S. H. Seismic structure of the southern Cascadia subduction zone and accretionary prism north of the Mendocino triple junction. *J. Geophys. Res.* **103**, 27207–27222 (1998).
14. Yuan, T., Spence, G. D. & Hyndman, R. D. Seismic velocities and inferred porosities in the accretionary wedge sediments at the Cascadia margin. *J. Geophys. Res.* **99**, 4413–4427 (1994).
15. Cochrane, G. R., Moore, J. C., Mackay, M. E. & Moore, G. F. Velocity and inferred porosity model of the oregon accretionary prism from multichannel seismic-reflection data — implications on sediment dewatering and overpressure. *J. Geophys. Res.* **99**, 7033–7043 (1994).
16. Cochrane, G. R., Moore, C. J. & Lee, H. J. In *Subduction Top to Bottom* (eds Bebout, G. E., Scholl, D. W., Kirby, S. H., & Platt, J. P.) 57-64 (American Geophysical Union, Washington, DC, 1996).
17. Carbotte, S. M. et al. Evolution and hydration of the Juan de Fuca crust and uppermost mantle: a plate-scale seismic investigation from ridge to trench. *AGU Fall Meeting Abstracts* **1**, 01 (2012).
18. Han, S. et al. Seismic reflection imaging of the Juan de Fuca plate from ridge to trench: new constraints on the distribution of faulting and evolution of the crust prior to subduction. *J. Geophys. Res.* **121**, 1849–1872 (2016).

19. Saffer, D. M. & Bekins, B. A. An evaluation of factors influencing pore pressure in accretionary complexes: implications for taper angle and wedge mechanics. *J. Geophys. Res.* **111**, B04101 (2006).
20. Saffer, D. M., Underwood, M. B. & McKiernan, A. W. Evaluation of factors controlling smectite transformation and fluid production in subduction zones: Application to the Nankai Trough. *Isl. Arc* **17**, 208–230 (2008).
21. Moore, J. C., Moore, G. F., Cochrane, G. R. & Tobin, H. J. Negative-polarity seismic reflections along faults of the Oregon accretionary prism — indicators of overpressuring. *J. Geophys. Res.* **100**, 12895–12906 (1995).
22. Davis, D., Suppe, J. & Dahlen, F. A. Mechanics of fold-and-thrust belts and accretionary wedges. *J. Geophys. Res.* **88**, 1153–1172 (1983).
23. Saffer, D. M. & Tobin, H. J. Hydrogeology and mechanics of subduction zone forearcs: fluid flow and pore pressure. *Annu. Rev. Earth Planet. Sci.* **39**, 157–186 (2011).
24. Saffer, D. M. & Wallace, L. M. The frictional, hydrologic, metamorphic and thermal habitat of shallow slow earthquakes. *Nat. Geosci.* **8**, 594–600 (2015).
25. Wannamaker, P. E. et al. Segmentation of plate coupling, fate of subduction fluids, and modes of arc magmatism in Cascadia, inferred from magnetotelluric resistivity. *Geochem. Geophys. Geosyst.* **15**, 4230–4253 (2014).
26. Scholz, C. H. Earthquakes and friction laws. *Nature* **391**, 37–42 (1998).
27. Kodaira, S. et al. High pore fluid pressure may cause silent slip in the Nankai Trough. *Science* **304**, 1295–1298 (2004).
28. Wallace, L. M. et al. Characterizing the seismogenic zone of a major plate boundary subduction thrust: Hikurangi Margin, New Zealand. *Geochem. Geophys. Geosyst.* **10**, Q10006 (2009).
29. Eberhart-Phillips, D., Reyners, M., Chadwick, M. & Chiu, J.-M. Crustal heterogeneity and subduction processes: 3-D *Vp, Vp/Vs* and *Q* in the southern North Island, New Zealand. *Geophys. J. Int.* **162**, 270–288 (2005).
30. Heise, W. et al. Changes in electrical resistivity track changes in tectonic plate coupling. *Geophys. Res. Lett.* **40**, 5029–5033 (2013).
31. Dean, S. M. et al. Contrasting decollement and prism properties over the Sumatra 2004–2005 earthquake rupture boundary. *Science* **329**, 207–210 (2010).
32. Gulick, S. P. S. et al. Updip rupture of the 2004 Sumatra earthquake extended by thick indurated sediments. *Nat. Geosci.* **4**, 453–456 (2011).
33. Henstock, T. J., McNeill, L. C. & Tappin, D. R. Seafloor morphology of the Sumatran subduction zone: surface rupture during megathrust earthquakes? *Geology* **34**, 485–488 (2006).
34. Hüpers, A. et al. Release of mineral-bound water prior to subduction tied to shallow seismogenic slip off Sumatra. *Science* **356**, 841–844 (2017).
35. Pichon, X. L., Henry, P. & Lallemant, S. Accretion and erosion in subduction zones: the role of fluids. *Annu. Rev. Earth Planet. Sci.* **21**, 307–331 (1993).
36. Tréhu, A. M., Blakely, R. J. & Williams, M. C. Subducted seamounts and recent earthquakes beneath the central Cascadia forearc. *Geology* **40**, 103–106 (2012).
37. Goldfinger, C., Kulm, L. D., McNeill, L. C. & Watts, P. Super-scale failure of the southern Oregon Cascadia margin. *Pure Appl. Geophys.* **157**, 1189–1226 (2000).
38. Morgan, J. K. & Bangs, N. L. Recognizing seamount-forearc collisions at accretionary margins: insights from discrete numerical simulations. *Geology* **45**, 635–638 (2017).
39. Bell, R. et al. Seismic reflection character of the Hikurangi subduction interface, New Zealand, in the region of repeated Gisborne slow slip events. *Geophys. J. Int.* **180**, 34–48 (2010).
40. Gutscher, M.-A., Klaeschen, D., Flueh, E. & Malavieille, J. Non-Coulomb wedges, wrong-way thrusting, and natural hazards in Cascadia. *Geology* **29**, 379–382 (2001).
41. Cubas, N., Souloumiac, P. & Singh, S. C. Relationship link between landward vergence in accretionary prisms and tsunami generation. *Geology* **44**, 787–790 (2016).
42. Zhou, J., Zhang, B. & Xu, Q. Effects of lateral friction on the structural evolution of fold-and-thrust belts: insights from sandbox experiments with implications for the origin of landward-vergent thrust wedges in Cascadia. *Geol. Soc. Am. Bull.* **128**, 669–683 (2016).
43. McNeill, L. C. & Henstock, T. J. Forearc structure and morphology along the Sumatra–Andaman subduction zone. *Tectonics* **33**, 112–134 (2014).
44. Ikari, M. J., Saffer, D. M. & Marone, C. Effect of hydration state on the frictional properties of montmorillonite-based fault gouge. *J. Geophys. Res.* **112**, B06423 (2007).
45. Kulm, L. D. & von Huene, R. et al. *Initial Reports of the Deep Sea Drilling Project* Volume 18 (US Government Printing Office, Washington DC, 1973).
46. Westbrook, G. K., Carson, B. & Musgrave, R. J. et al. Cascadia margin sites 888–892. In *Proc. ODP Sci. Res.* (Ocean Drilling Program, Texas, 1994); https://doi.org/10.2973/odp.proc.ir.146-1.1994
47. Davis, E. E. et al. Hydrothermal circulation in the oceanic crust: eastern flank of the Juan de Fuca Ridge: sites 1023–1032. In *ODP Sci. Res.* Vol. 168 (Ocean Drilling Program, Texas, 1997); https://doi.org/10.2973/odp.proc.ir.168.1997

Acknowledgements

We thank the captain, crew and technical staff of R/V *Marcus G. Langseth* for their efforts, which made the success of cruise MGL1211 possible. Seismic data processing and interpretation was conducted using the Paradigm processing software packages Echos and Geodepth. We thank A. Arnulf for providing the velocity profile from the Hikurangi margin. This research was supported by the National Science Foundation through a GeoPRISMS Postdoctoral Fellowship (Award 1457221) to S.H. and Award 1029411 to S.M.C.

Author contributions

S.H. participated in the data collection and processed the seismic data. S.M.C. conceived of the project and led the data collection. S.H., N.L.B. and S.M.C interpreted the seismic data. S.H. and D.M.S. conducted the porosity and effective stress analysis. J.C.G. participated in the data collection and provided the starting models for velocity analysis. S.H. wrote the paper with contributions and edits from all other authors.

Competing financial interests

The authors declare no competing financial interests.

Additional information

Supplementary information is available for this paper at https://doi.org/10.1038/s41561-017-0007-2.

Reprints and permissions information is available at www.nature.com/reprints.

Correspondence and requests for materials should be addressed to S.H.

Publisher's note: Springer Nature remains neutral with regard to jurisdictional claims in published maps and institutional affiliations.

Methods

Seismic data processing, interpretation and uncertainty estimation of seismic velocities. The acquisition parameters of the multichannel seismic data are described in detail in ref. [18]. We conducted two-dimensional Kirchhoff pre-stack depth migration (PSDM) on the WA and OR transects from ~45 km seaward to ~25 km landward of the deformation front and on the MARGIN transect to characterize the deformation styles and velocity structures of the sediments near the deformation front (Figs. 1–3 and Supplementary Fig. 1). Pre-processing of the multichannel seismic data includes: geometry definition to bin the data into 6.25-m-spaced common mid-point gathers; band-pass filtering (3–7–220–250 Hz) to remove cable noise; trace editing; spherical divergence correction; resampling to 4 ms; despiking; radon filtering to remove the seafloor multiple; predictive deconvolution to collapse the airgun source bubble-pulse reverberations. Velocity models from pre-stack time migration[18] are used as starting models for Kirchhoff PSDM and are updated using semblance analysis at 312.5–625 m spacing (on every 50–100 common reflection point gathers) along the WA and OR transects and every 1,250 m (200 common reflection points) along the MARGIN transect (Supplementary Fig. 4). The final velocity models converge to a stable solution by 5–10 iterations. The full-extent PSDM images of sediments near the deformation front on the WA and OR transect are shown in Supplementary Fig. 1.

Faults in the sediment sections are interpreted from the offsets of sediment layers and fault-plane reflections. The stratigraphic horizon where frontal thrust faults stop at or merge into is interpreted as the décollement. Beneath the Hydrate Ridge on the OR transect where the noise level is relatively high, the décollement is determined by tracing the relatively bright reflection segments following the projection of the horizon. Along our OR transect, the décollement develops at the boundary between Astoria Fan turbidites and abyssal plain turbidites. This stratigraphic boundary is constrained by Deep Sea Drilling Program Site 174[45] and is traced from an unconformity in the sediment section ~ 75 km seaward of the deformation front along the OR transect[18].

We estimate the uncertainty of our velocity model by adding velocity perturbations as a percentage of the original velocity to a layer of certain thickness at different depths of the velocity profile. In this way, we can estimate the size and amplitude of the anomaly that can result in detectable deviation of the semblance from the zero line (Supplementary Fig. 5). Using this approach, velocity uncertainties are estimated to be within 5% for locations seaward of the deformation front and can be up to 15% in the accretionary wedge. The velocities at the crossings of WA, OR and MARGIN transects are in good agreement (Supplementary Fig. 6).

Calculation of reference velocity. We define a reference velocity to represent the normal consolidation state (uniaxial deformation in the vertical direction, pore fluid pressure equivalent to hydrostatic pressure) of sediments on top of the Juan de Fuca Plate offshore Washington and Central Oregon (Supplementary Fig. 2a–c), and use the deviation from the reference velocity (that is, residual velocity) to characterize the under- or over-consolidation of sediments near the deformation front (Figs. 2 and 3). The purpose of the reference velocity is mainly to compare consolidation states and reveal systematic along-strike variations in the relative consolidation state of the initially similar sediment sequences offshore Washington and Central Oregon. The reference velocity is obtained by averaging vertical seismic velocity profiles from 40–45 km seaward of the deformation front along the WA and OR transects where the sediments are assumed to be well drained. The reference velocity is in good agreement with log-sonic velocity measurement from ocean drilling sites 1032 and 888 on the incoming Juan de Fuca Plate[46,47] (within ±2% of the reference velocity for the depth range <350 m, and within ± 5% for depths of 350–500 m) (Supplementary Fig. 2c). To extend the reference velocity beyond the maximum depth (~1,460 m) of the sediment section at the reference location, we compiled and compared sediment velocities from margins with thick incoming sediment sequences and sedimentary basins (Makran[48], Sumatra[49], Hikurangi[50], Alaska[51] and Los Angeles basin[52], Supplementary Fig. 2a) and used seismic velocities measured for abyssal sediments at the Makran margin to extend the reference velocity to ~5,500 m. From 5,500 to 7,000 m, we used a linear extrapolation (Supplementary Fig. 2b). We adopt the velocity profile from the Makran margin to represent our reference velocity at depths >1.5 km for the following reasons: the topmost 1.2 km of the Makran velocity profile matches our seismic-derived velocity in the same depth range very well; thus, the effects of other factors, such as differences in sedimentation rates and lithology, are likely to be secondary; the smooth-varying velocity gradient versus depth suggests that the effect of lithology changes on seismic velocity is minimal (the Hikurangi and Alaska–Pacific velocity profiles show distinct velocity gradients in the shallow and deep parts, suggesting major effects of lithological changes) (Supplementary Fig. 2a); recent geophysical studies have found that the deep stratigraphic section of Makran sediments is generally well drained despite a high sedimentation rate, and thus it is a good representation for normal consolidation[53].

Porosity and effective stress analysis. Within the span of our seismic transects, the sediment section is composed of Pliocene to recent turbidites derived from Astoria Fan and Nitinat Fan overlying a silty turbidite and hemipelagic unit deposited in the near-ridge and plate-interior setting, as documented by numerous drilling efforts[45–47,54,55]. Although variations in the clay content are documented in the near-surface sediments, there is no evidence that these variations extend into the basal sediments near the deformation front offshore Washington and Oregon[54], where a large velocity difference is observed in our study. Furthermore, in the distance range 30–45 km seaward of the deformation front, near our reference sites, the velocity structure of Washington and Oregon is very similar. Therefore, we consider the effect of lithological variation to be minimal, and attribute the near-deformation-front seismic velocity variations observed along our transects to changes in consolidation state and porosity.

We follow an approach similar to that of refs [56,57] to derive porosity and in situ effective stress from seismic velocity. We first compile V_p and porosity (ϕ) measurements from logging and core data at ocean drilling sites that are seaward of the deformation front with penetration depths >500 m, and outside the highly active hydrothermal circulation zone near the Juan de Fuca Ridge (Supplementary Table 2). The compiled data are compared with different empirical relationships[58–60] (Supplementary Fig. 7). The H&T04[60] relationship fits the Cascadia data well and has a wide V_p range spanning our measured velocities, and thus is chosen to convert our PSDM V_p models to porosity.

We then derive an empirical relationship between porosity and mean effective stress at the reference site. The converted porosity–depth profile (Supplementary Fig. 8a) at the reference site is fitted with Athy's relationship.

$$\phi = \phi_0 exp(-bz) \tag{1}$$

where ϕ_0 is the porosity of material at the surface, b is the compaction constant dependent on the lithology and geological settings, and z is depth (m). The best fitting parameters are $\phi_0 = 0.4774$; $b = 0.0004601$.

With these parameters, we use equation (5) in ref. [57] to calculate the vertical effective stress (σ_z').

$$\sigma_z' = \frac{(\rho_s - \rho_f)g}{b}\left[\left(ln\ \phi_0 - \phi_0\right) - (ln\ \phi - \phi)\right] \tag{2}$$

where g is the gravitational acceleration (m s^{-2}), and ρ_s and ρ_f are the solid grain and fluid densities (kg m^{-3}), respectively. At the reference site, the sediments are under normal consolidation conditions ($\sigma_1' > \sigma_2' = \sigma_3'$, $\sigma_z' = \sigma_1'$, where σ'_1, σ'_2, and σ'_3 are the maximum, intermediate, and minimum principal effective stress, respectively). Thus, we can use equation (3) to calculate mean effective stress (σ_m'). An experimentally determined ratio between minimum and maximum principal effective stress $R = 0.6$ (ref. [61]) is applied.

$$\sigma_m' = \frac{\sigma_1' + \sigma_2' + \sigma_3'}{3} = \frac{(1+2R)}{3}\sigma_z',\ R = \frac{\sigma_3'}{\sigma_1'} \tag{3}$$

While differential stress (or stress path) is known to affect porosity, mean stress is the dominant control[62,63]. Therefore, we convert the porosity to mean effective stress along the WA and OR transects using the relationship derived at the reference sites.

Compilation of décollement depth. To examine the relationship between the décollement depth and the velocity of the basal sediments seaward of the deformation front, we compile information from existing seismic studies on the depth of the décollement near the deformation front from 44.3° N to 47.8° N along the Cascadia margin (Supplementary Table 1). The décollement on the time- or depth-migrated seismic images of the previously published seismic lines is digitized according to the interpretations in the reference. For ORWELL line 103[11], we disagree with the authors' interpretation, and include the depth of our interpreted décollement besides the original interpretation in Supplementary Table 1. On OR-18 and OR-01[10] where only two-way travel time of the décollement depth is available, we convert the two-way travel time between décollement and basement to thickness using the average interval velocity between the décollement and the basement from our nearby OR transect.

Data availability. All multichannel seismic field data, seismic navigation and acquisition logs are archived with the IEDA: Marine Geoscience Data System (https://doi.org/10.1594/IEDA/319000). PSDM images and velocity models are available from the corresponding author upon request.

References

48. Minshull, T. & White, R. Sediment compaction and fluid migration in the Makran accretionary prism. *J. Geophys. Res.* **94**, 7387–7402 (1989).
49. Qin, Y. & Singh, S. C. Detailed seismic velocity of the incoming subducting sediments in the 2004 great Sumatra earthquake rupture zone from full waveform inversion of long offset seismic data. *Geophys. Res. Lett.* **44**, 3090–3099 (2017).
50. Arnulf, A. F. Structure and physical characteristics of the Southern Hikurangi Subduction Zone derived from seismic full waveform imaging. *Seismol. Res.* Lett. **88**, 656 (2017)

51. Christeson, G. L. et al. The Yakutat terrane: dramatic change in crustal thickness across the Transition fault, Alaska. *Geology* **38**, 895–898 (2010).
52. Süss, M. P. & Shaw, J. H. P wave seismic velocity structure derived from sonic logs and industry reflection data in the Los Angeles basin, California. *J. Geophys. Res.* **108**, 2170 (2003).
53. Smith, G., McNeill, L., Henstock, T. J. & Bull, J. The structure and fault activity of the Makran accretionary prism. *J. Geophys. Res.* **117**, B07407 (2012).
54. Underwood, M. B. Strike-parallel variations in clay minerals and fault vergence in the Cascadia subduction zone. *Geology* **30**, 155–158 (2002).
55. Underwood, M. B. et al. Provenance, stratigraphic architecture, and hydrogeologic influence of turbidites on the mid-ocean ridge flank of northwestern Cascadia Basin, Pacific Ocean. *J. Sediment. Res.* **75**, 149–164 (2005).
56. Tobin, H. J. & Saffer, D. M. Elevated fluid pressure and extreme mechanical weakness of a plate boundary thrust, Nankai Trough subduction zone. *Geology* **37**, 679–682 (2009).
57. Skarbek, R. M. & Saffer, D. M. Pore pressure development beneath the decollement at the Nankai subduction zone: implications for plate boundary fault strength and sediment dewatering. *J. Geophys. Res.* **114**, B07401 (2009).
58. Hyndman, R. D., Moore, G. F. & Moran, K. Velocity, porosity, and pore-fluid loss from the Nankai subduction zone accretionary prism. In *Proc. ODP Sci. Res.* (eds Hill, I. A. et al.) Vol. 131, 211–220 (Ocean Drilling Program, Texas, 1993); https:doi.org/10.2973/odp.proc.sr.131.125.1993
59. Erickson, S. N. & Jarrard, R. D. Velocity-porosity relationships for water-saturated siliciclastic sediments. *J. Geophys. Res.* **103**, 30385–30406 (1998).
60. Hoffman, N. W. & Tobin, H. J. An empirical relationship between velocity and porosity for underthrust sediments in the Nankai Trough accretionary prism. In *Proc. ODP Sci. Res.* Vol. 190/196 (Ocean Drilling Program, Texas, 2004); https://dx.doi.org/10.2973/odp.proc.sr.190196.355.2004
61. Karig, D. E. & Hou, G. High-stress consolidation experiments and their geologic implications. *J. Geophys. Res.* **97**, 289–300 (1992).
62. Wood, D. M. *Soil Behaviour and Critical State Soil Mechanics* (Cambridge Univ. Press, Cambridge, 1990).
63. Kitajima, H. & Saffer, D. M. Elevated pore pressure and anomalously low stress in regions of low frequency earthquakes along the Nankai Trough subduction megathrust. *Geophys. Res. Lett.* **39**, L23301 (2012).